ACS OMEGA

http://pubs.acs.org/journal/acsodf

Article

# Bijels as a Fluid Labyrinth for Drugs: The Effect of Nanoparticles on the Release Kinetics of Ethosuximide and Dimethyl Fumarate

Valeria Vanoli, Giovanna Massobrio, Fabio Pizzetti, Andrea Mele, Filippo Rossi,* and Franca Castiglione*

Cite This: *ACS Omega* 2022, 7, 42845−42853

Read Online

ACCESS | Metrics & More | Article Recommendations | Supporting Information

**ABSTRACT:** Bijels (bicontinuous interfacially jammed emulsion gels) raised an increasing interest as biomaterials for controlled drug delivery due to their biphasic nature organized in mesoscopic tortuous domains. Two bijel formulations were prepared and explored as delivery systems for both hydrophilic and lipophilic drugs, ethosuximide and dimethyl fumarate. The two bijel-like structures, based on polymerized ε-caprolactone/water, differ in the stabilizing nanoparticle hydroxyapatite (inorganic) and nanogel-based nanoparticles (organic). Diffusion nuclear magnetic resonance spectroscopy has been used to characterize the bijel structure and the transport behavior of the drug molecules confined within the water/organic interconnected domains. A reduced diffusion coefficient is observed for several concentrations of the drugs and both bijel formulations. Moreover, *in vitro* release profiles also reveal the effect of the microstructure and drug−nanoparticle interactions.

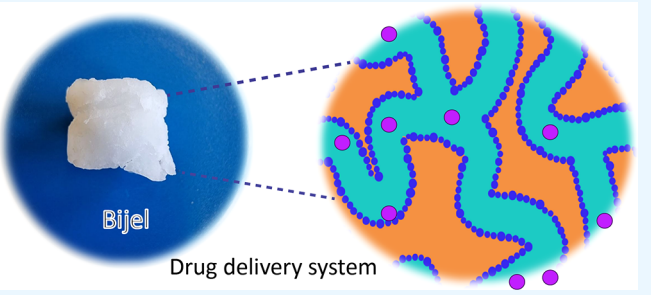




## 1. INTRODUCTION

Bicontinuous interfacially jammed emulsion gels (known as "bijels") are a new class of soft materials composed of two nonmiscible fluids, such as water and oil, confined in a bicontinuous morphology by a monolayer of colloidal nanoparticles with equal affinity for the two fluids.[1−3] The simultaneous presence of interconnected polar and apolar domains makes these materials suitable for several technological applications including molecular encapsulation,[4,5] tissue engineering,[6−9] and cosmetic[10,11] and drug delivery.[12−15] The latter is one of the most relevant applications as due to the biphasic nature of these materials, they are able to carry and release both lipophilic and hydrophilic drugs in the same system. Similarly to organogels[16,17] and hydrogles,[18,19] also developed as platforms for the controlled release of active ingredients or vaccines through a variety of different formulations,[20] it is possible to fine-tune the structural/release properties by adjusting the preparation conditions. The design and fabrication of a bijel-like structure relay on a careful control of several key physical parameters, such as the liquid−liquid surface tension, the size of the nanoparticles, their symmetric wettability by the two liquids, and the characteristic time for jamming the interface.[21] The interfacial self-assembly of colloidal particles or nanoparticles (NP) at a liquid−liquid interface due to NP-liquid favorable interactions minimizes the free energy of the system and leads to the formation of jammed structures.[22] In particular, the channel width of the biphasic domains can be systematically varied by modifying the radius, volume fraction, and concentration of the colloidal particles[23] and/or nanoparticles.[24,25] Several theoretical calculations have been performed to study the interplay of all these factors in obtaining stable biphasic bicontinuous structures. Jansen and Harting,[26] using the multi-phase lattice Boltzmann method, demonstrated that the fluid ratio and particle wettability have a crucial effect on the formation of bijel-like structures versus Pickering emulsions. Subsequent simulations[27] have shown how the extent of particle−particle interactions, particle wettability, size, and diffusion determines the microstructure of the bijels in bulk samples and thin fluid films.[28]

Recently, several experimental methodologies for preparing the bijel-like structure have been proposed. They are essentially based on two synthesis paths: (i) by quenching partially immiscible liquids such as alcohol/alkane or 2,6-lutidine/water to induce phase separation via spinodal decomposition[1−3] and (ii) by inducing phase separation in oil/water mixtures and stabilizing the fluid−fluid interfaces using colloidal particles, nanoparticles,[29] or a combination of nanoparticles and molecular surfactants.[8] In this process, both the shape of the nanoparticles, spherical shape[8,30] or rod-like

Received: July 30, 2022
Accepted: October 26, 2022
Published: November 16, 2022

nanoparticles,[31] and the particle surface properties define the morphology of the bijel-like structures. Furthermore, particle−fluid and inter-particle interactions, due to colloidal forces, *e.g.*, van der Waals attraction and electrostatic and steric repulsion, must also be considered in the design of the bijel formation pathways.

In our study, a bijel-like network based on polymerized ε-caprolactone/water[32] and stabilized by polyethylene glycol (PEG)-Jeffamine nanogel (organic nanoparticles) is prepared and its structure, morphology, and stability are characterized for the first time. Moreover, we investigate the effect induced by two different colloidal nanoparticles: porous hydroxyapatite (HAp) and PEG-Jeffamine nanogel (NG) on the properties/morphology of these bijels as drug delivery systems. Regarding this application, we consider here two active pharmaceutical ingredients: (i) ethosuximide, a water-soluble drug used extensively in the treatment of epilepsy conditions[33] and (ii) dimethyl fumarate, a drug with low solubility in water used to treat psoriasis,[34] relapsing forms of multiple sclerosis (MS) and relapsing remitting MS (RRMS).[35] The chemical structure of both drugs is displayed in Scheme 1.

**Scheme 1. (a) Ethosuximide and (b) Dimethyl Fumarate Chemical Structure**

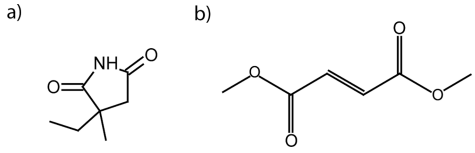


The transport properties of both hydrophilic/lipophilic small drugs loaded in the water/organic bijel phases and the drug−nanoparticle interactions are investigated at the molecular level using high-resolution magic angle spinning (HR-MAS) diffusion nuclear magnetic resonance (NMR) techniques[36−39] suitable for soft materials and gels also in the presence of nanoscale confinement.[40] In particular, we consider the effect of the nanoparticle type and drug concentration on their transport properties in the bijel fluid network. Finally, the NMR results for drug diffusion are compared with the macroscopic release kinetics by the two biphasic porous materials. Our interest in the development of bijel-like materials is motivated by the importance of multi-drug delivery systems.

## 2. EXPERIMENTAL SECTION

**2.1. Materials.** Calcium hydroxide ($Ca(OH)_2$, ≥98%) and orthophosphoric acid ($H_3PO_4$, ≥85%) were purchased by Carlo Erba Reagents (Carlo Erba Reagents, Milano, Italy). ε-Caprolactone (CL, ≥99%) and 1,5,7triazabicyclo[4.4.0]dec-5-ene (TBD, ≥ 95%) were purchased by Sigma-Aldrich, Germany. Arabic gum (AG) was kindly gifted from the research group of Prof. Ciofani from Scuola Superiore di Studi Universitari e Perfezionamento Sant'Anna, CRIM Lab-Center for Applied Research in Micro and Nano Engineering. Jeffamine (Elastamine RE-2000) was sold by Huntsman Corporation (Woodlands, Texas, USA). Polyethylene glycol 8000 (PEG8000, MW = 8 kDa), carbodiimidazole (CDI, ≥ 98%), deuterium oxide (99.9 atom % D), PBS (Dulbecco's phosphate-buffered saline solution pH = 7.4, 0.1 M), ethosuximide (Etho, MW = 141.168 g/mol), and dimethyl fumarate (DMF, MW = 144.127 g/mol) were purchased from Sigma-Aldrich, Germany. Fluorescein sodium salt (SF, MW = 412.3 g/mol) and rhodamine B (RhB, MW = 479.02 g/mol) were purchased from Merck (Deisenhofen, Germany). All reagents and solvents were used without further purification. Solvents were of analytical laboratory grade. Synthetized products were stored at 4 °C in the dark until used.

**2.2. Materials Synthesis.** *2.2.1. Hydroxyapatite Nanoparticle (HAp) Synthesis.* Hydroxyapatite nanoparticles were synthesized according to the procedure reported by Kumar *et al.*[41] A 0.2 M solution of $Ca(OH)_2$ dissolved in distilled water (24.9 mL) was stirred at 400 rpm and heated at 100 °C for 1 h. Then, a 0.12 M solution of $H_3PO_4$ (0.2 mL) was added to the water solution at a controlled rate of 4 mL/min using a dripping funnel. At the end of the addition, the pH was checked to be near neutrality with a litmus test and the mixture was left reacting for 2 h. After resting overnight, the solution underwent five centrifugation cycles at 5000 rpm of 3 min each, with supernatant removal and particle dispersion between each of them. The product was dried at 200 °C in an oven for 6 h and manually grinded with a pestle. The hydroxyapatite appears as a white fine powder, and the yield was 301 mg (81%). To stabilize nanoparticle dispersion preventing aggregation, a solution of Arabic gum (AG) in distilled water was heated at 37 °C for 1 h under moderate stirring and was successively added to the nanoparticles to achieve a 1:1 weight ratio.

The dispersion was sonicated for 12 h in an ultrasonic bath (Bandelin Sonorex) to make the AG graft onto the NP surface. Several colloidal dispersions of HAp were stabilized at a concentration of 20 mg/mL. For each of them, the DLS analysis was employed to evaluate the NP diameter.

*2.2.2. PEG-Jeffamine Nanoparticle (NG) Synthesis.* A solution of Jeffamine (2.5 g, 1.25 mmol) in $H_2O$ (5 mL) was added dropwise to a stirred solution of PEG-CDI (1 g, 0.125 mmol) in DCM (3 mL). The mixture was sonicated with a bath sonicator for 30 min at room temperature to obtain nanogels (NGs) and left stirring overnight in an open flask to let the DCM evaporate. The result was dialyzed against distilled water in an RC membrane with a 3.5 kDa cutoff for 72 h. Finally, the dialyzed product was lyophilized for 72 h, until all the remaining water was removed. The overall process is represented in Figure 1, and the yield was 0.706 g (70%). DLS analysis was performed to evaluate the hydrodynamic radius.

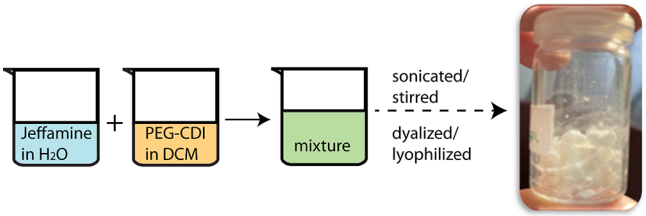


**Figure 1.** Schematic representation of PEG-Jeffamine nanoparticle synthesis.

*2.2.3. Bijel Preparation.* A catalytic amount of TBD (12.5 mg) was added to a mixture of ε-caprolactone/ethanol (0.5 mL/55 μL), as reported by Marino *et al.*[42] The solution was mixed at 1000 rpm for 8−15 min. Subsequently, 375 μL of the colloidal dispersions (the HA- or the NG-based one) was added, and the shaking speed was increased to 1700 rpm for 40 s to reassure a good distribution before the speed was reduced back to 1000 rpm until the complete polymerization was


https://doi.org/10.1021/acsomega.2c04834
ACS Omega 2022, 7, 42845−42853

reached. As a container for the sample, a syringe (volume of 6 mL) with one end severed was chosen to extrude the sample without breaking its structure. The bijel preparation pathway is shown in Figure 2. The final morphological and structural features will be assessed by scanning electron microscopy, differential scanning calorimetry, and $^{1}$H HR-MAS NMR spectroscopy.

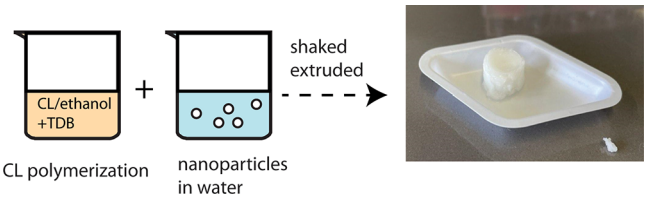


**Figure 2.** Schematic representation of the bijel preparation pathway.

*2.2.4. Bijel Drug Loading.* Ethosuximide (Etho) and dimethyl fumarate (DMF) were chosen as loading drugs for the aqueous phase and for the organic phase, respectively.

*2.2.4.1. Samples for HR-MAS NMR Spectroscopy.* The hydrophilic drug was dissolved directly in the aqueous solution of NPs, whereas the hydrophobic one was added to the caprolactone prior to polymerization. Ethosuximed-loaded bijels having drug concentrations of 25, 50, and 100 mg/mL were prepared. Dimethyl fumarate-loaded bijels were separately prepared with two different drug concentrations of 12.5 and 25 mg/mL. The two drugs Etho and DMF were loaded into the bijels at different concentrations due to their diverse solubility in the water/organic phase. Given the high solubility of Etho in water (190 g/L at 25 °C), it was possible to load the bijels with three different concentrations of the drug and because the solubility of DMF in $\varepsilon$-caprolactone is lower, it was possible to prepare the bijels loaded with only two lower drug concentrations.

*2.2.4.2. Samples for Release Tests.* Hydrophilic drug-mimetic compounds (fluorescein sodium salt and rhodamine B) and ethosuximide were dissolved in the aqueous phase with a concentration of 1 mg/mL, and dimethyl fumarate was also dissolved in caprolactone (1 mg/mL). Afterward, the bijel synthesis was carried out following the procedure just described.

**2.3. Sample Preparation.** *2.3.1. Solution State NMR Spectroscopy.* Several liquid solutions composed by ethosuximide dissolved in $D_2O$ at various concentrations (C1 = 25, C2 = 50, and C3 = 100 mg/mL) and dimethyl fumarate dissolved in caprolactone at various concentrations (C4 = 12.5 and C5 = 25 mg/mL) were prepared for NMR analysis. The solutions were transferred in a 5 mm NMR tube.

**2.4. Measurements.** *2.4.1. Dynamic Light Scattering (DLS).* DLS measurements were performed with a Malvern Zetasizer Nano ZS at a scattering angle of 173° (backscatter) to identify the hydrodynamic diameters and the polydispersity index (PDI) of the NPs produced. The temperature was kept at 25 °C, and an equilibration time of 20 s was provided before each measurement. Each sample was analyzed three times, and the results were averaged.

*2.4.2. Scanning Electron Microscopy (SEM).* Environmental scanning electron microscopy analysis was performed on gold-sputtered samples at 10 kV with Evo 50 EP instrumentation (Zeiss, Jena, Germany). To preserve the actual morphology of the product, freeze-drying (for 150 h) was applied to remove all the liquid phases by sublimation. With this technique, the polymer chains are expected to retain the same conformation they had in wet conditions.

*2.4.3. Differential Scanning Calorimetry (DSC).* Thermal property analysis was performed on a Mettler Toledo DSC polymer machine calibrated with indium and zinc standards. The heating rate was 10 °C/min under nitrogen flow. The melting point and glass transition temperature were derived from the first heating curve.

*2.4.4. NMR Spectroscopy.* The $^{1}$H HR-MAS NMR spectra of each gel sample were recorded using a Bruker Avance DRX spectrometer operating at 500 MHz proton frequency, equipped with a dual $^{1}$H/$^{13}$C high-resolution magic angle spinning (HR-MAS) probe head for semisolid samples. This approach relies on the fast rotation of the sample at the magic angle ($\theta$ = 54.78° with respect to the $z$ direction of the stray field of the NMR magnet), which averages the dipole−dipole interactions and susceptibility distortions, allowing to record spectra with high resolution. The bijel sample was carefully transferred in a 4 mm $ZrO_2$ rotor (12 $\mu$L volume), ensuring that the gel texture was not destroyed. All the $^{1}$H HR-MAS spectra were acquired with a spinning rate of 4 kHz. The $^{1}$H NMR spectra of the liquid samples were also recorded by using a conventional high-resolution NMR probe and standard 5 mm glass NMR tubes. The temperature was set and controlled at 305 K with an air flow of 535 L·h$^{-1}$ to avoid any temperature fluctuations due to sample heating during the magnetic-field pulse gradients.

Diffusion coefficients of the liquid and gel samples were measured using diffusion-ordered spectroscopy (DOSY) methods. The experiments were performed using the bipolar pulse longitudinal eddy current delay (BPPLED) pulse sequence.[43] A pulsed gradient unit to produce magnetic-field pulse gradients in the $z$ direction up to 53 G·cm$^{-1}$ was used. The durations of the magnetic-field pulse gradients ($\delta$) and the diffusion times ($\Delta$) were optimized for each sample to obtain complete dephasing of the signals with the maximum gradient strength. The acquisition parameters for variable observation time measurements were $\delta$ = 0.5−1.9 ms and $\Delta$ = 10−60 ms in a step of 10 ms; for all the other samples, $\Delta$ was set to 50 ms while the $\delta$ value was 1.7 ms. In each experiment, a series of 28 spectra with 16 K points were collected with a D1 relaxation delay of 10 s. The pulse gradients were increased from 2 to 95% of the maximum gradient strength in a linear ramp. Each experiment of the gel samples was repeated in triplicate.

*2.4.5. Release Studies.* The bijel drug-loaded samples were submerged in 2 mL of PBS (0.1 M, pH 7.4) and incubated at 30 °C. At time points of 5 min, 30 min, 1 h, 1 h and 30 min, 2 h, 3 h, 4 h, 6 h, 7.25 h, 24 h, and 32 h, 1000 $\mu$L of the released media was withdrawn for UV measurements (UV−vis spectrophotometer V-630). At each measure, 1000 $\mu$L of fresh PBS was added to maintain the volume. The released amount of drug was measured spectrophotometrically at the wavelength corresponding to the peak of absorbance (ethosuximide = 244 nm, dimethyl fumarate = 236 nm) and determined referring to the standard calibration curve for each of them. The Lambert−Beer law was used to construct the release curves, ensuring that the absorbance measured was always in the linear range. Each measurement was repeated three times. The release study of the fluorophore drug-like molecules was performed following the procedure described in ref 32.


https://doi.org/10.1021/acsomega.2c04834
ACS Omega 2022, 7, 42845−42853

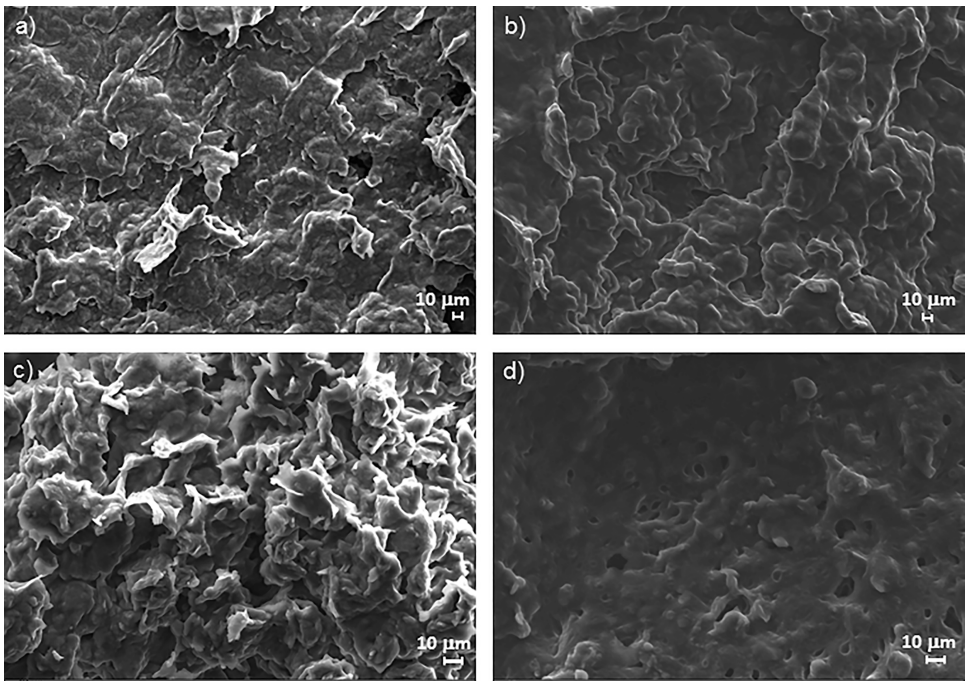


**Figure 3.** SEM images of the bijels/HAp (a, c) and bijels/NG (b, d) at different magnifications.

**Figure 4.** Nanogel-based samples at $t_0$, 6 h, 8 h, 24 h, 50 h, 1 week, and 2 weeks (from left to right). The tests have been carried out in quadruplicate.

## 3. RESULTS AND DISCUSSION

**3.1. Characterization of the Bijel-like Structures.** Several analytical techniques have been used to thoroughly investigate the morphology, properties, and behavior of the bijels produced with the two different nanoparticles HAp and NG.

*3.1.1. SEM.* Figure 3 shows SEM images useful for characterizing the internal morphology of the samples. The observed morphology is the result of the interpenetration of the organic and aqueous phase during the preparation of the samples. The resulting pores (darkest zones in the images) are originated by the removal of the aqueous phase during freeze-drying necessary to perform the SEM analysis. The internal structure of bijel/NG strongly resembles that of the matrix obtained with HAp nanoparticles. However, the structure of bijel/HAp is more jagged with respect to the other one, which presents smoother shapes. The particles are not directly observable in these pictures being of nanometric size.

*3.1.2. Thermal Properties.* The melting ($Tm$) and crystallization points ($Tc$) of the products have been investigated by performing DSC analyses: the results showed a $Tm$ of the two systems of 50 and 40 °C and $Tc$ of 25 and 19 °C for the bijel/HAp and bijel/NG samples, respectively (Figures S1 and S2). These are above physiological temperatures, indicating that both could be used as drug delivery systems without dissolving once injected. This has been further confirmed through stability tests that simulated body



https://doi.org/10.1021/acsomega.2c04834
ACS Omega 2022, 7, 42845−42853

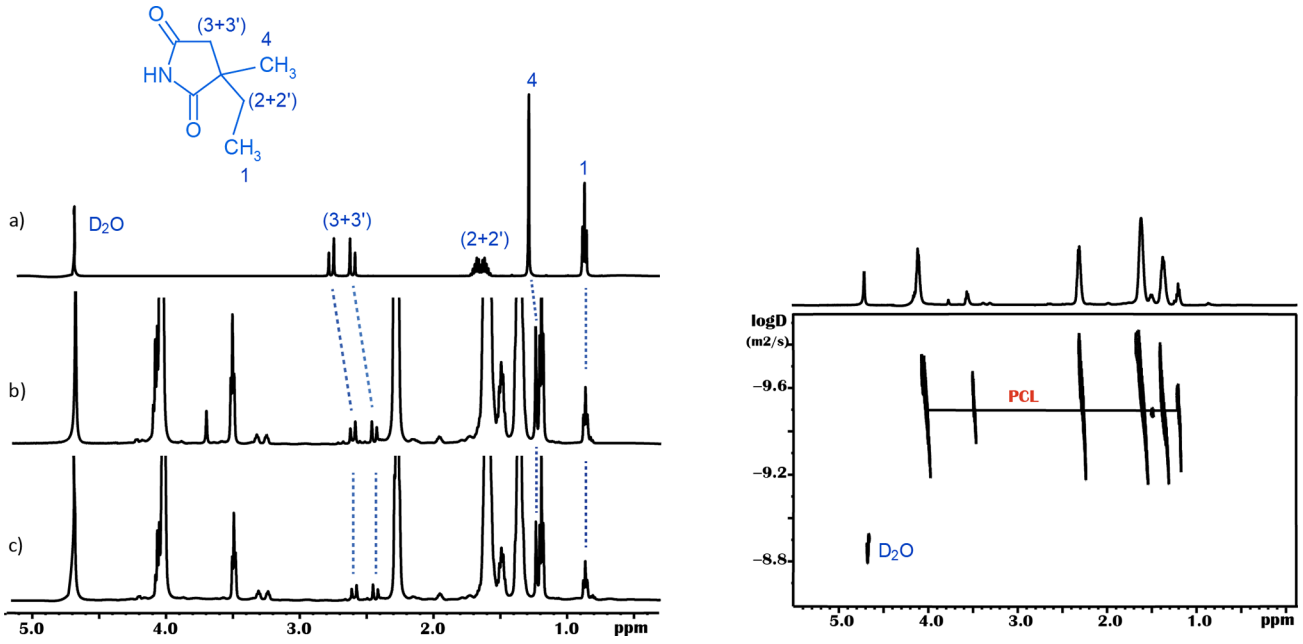


**Figure 5.** (Left panel) (a) $^1$H spectrum of ethosuximide dissolved in $D_2O$ and peak assignment; (b, c) $^1$H HR-MAS spectra of ethosuximide loaded in bijel/NG and bijel/HAp, respectively. (Right panel) $^1$H HR-MAS DOSY map of NG-based bijel.

conditions: both systems showed good resistance at 37 °C, lasting up to 2 weeks (see Figure 4).

*3.1.3. DLS.* DLS analyses were performed to evaluate NG nanoparticle dimensions and, therefore, their ability to stabilize a colloidal dispersion in water. The NG nanoparticles had a mean size dimension of 434.6 nm with a polydispersity index (PdI) of 0.6, while HAp nanoparticles had a mean size of 372.9 nm, PdI = 0.27 (Figures S3 and S4).

*3.1.4. HR-MAS NMR Structure and Diffusion.* HR-MAS NMR spectroscopy, due to the magic angle spinning set-up, allows us to obtain the high-resolution spectra of soft materials such as gels, thus enabling structural investigation of drug−polymer interactions together with the dynamic properties of the drug molecules loaded in the gel phase. The $^1$H HR-MAS spectra of ethosuximide-loaded bijel/HAp and bijel/NG are reported in Figure 5b,c together with the $^1$H spectrum of the drug dissolved in $D_2O$ (trace a) and peak assignment. The $^1$H HR-MAS spectra of the gel phase both show high-resolution sharp lines for all the species with some well-defined peaks of the drug (protons 1, (3 + 3′), and 4; see Figure 5 for atom labels). A comparison between the HR-MAS versus high-resolution spectra shows that, overall, the NMR spectrum of ethosuxymide is retained upon encapsulation of the drug in the bijel, meaning that no changes in the spin systems are observed. This finding confirms that the entrapment process does not alter the chemical structure of the drug, thus allowing its biological activity. Conversely, some selective chemical shift variations are observed in the NMR spectrum of ethosuximide in the bijel compared to the reference in $D_2O$. In particular, protons (3 + 3′) and 4 undergo an upfield chemical shift change (0.16 and 0.05 ppm, respectively), while no changes are observed for the methyl 1. These results suggest that the drug is likely to interact with the nanoparticle surface mainly via the heterocyclic ring through non-covalent interactions, which selectively change the magnetic environment of the mentioned protons without modification of the drug's molecular structure. The $^1$H HR-MAS spectra of dimethyl fumarate loaded in bijel/HAp and bijel/NG (Figure S5) also show chemical shift variations compared to the high-resolution spectrum. Moreover, no effects on the spectral features, due to the different stabilizing nanoparticles, are observed in the bijels.

DOSY NMR has been used to characterize the bijel-like structure and observe the diffusion motion of the drug molecules in the water/organic phases. The technique, based on the application of magnetic-field gradients, is able to encode the molecular motion by carrying out a set of experiments with a linearly increasing gradient pulse strength. The final output of the experiment is a 2D map encoding the chemical shift of the observed species in the horizontal axis versus their diffusion coefficient, $D$, in the vertical dimension.[44−46]

The signal attenuation, $I(q, \Delta)$, for a given interpulse delay, $\Delta$, is related to the gradient strength, $g$, and to the mean square displacement (MSD), $\langle z^2 \rangle$, of each diffusing species according to

$$I(q, \Delta) = I_0(0, \Delta)e^{-1/2q^2\langle z^2 \rangle} \quad (1)$$

where $q = (\gamma g \delta)/2\pi$, $\gamma$ is the gyromagnetic ratio of the observed nucleus, and $\delta$ is the length of the gradient pulse. For isotropic solutions, the mean square displacement shows a linear dependency with diffusion time $\Delta$, as given by the equation

$$\langle z^2 \rangle = 2D\Delta \quad (2)$$

where $D$ is the diffusion coefficient. The above equation holds strictly for unrestricted Gaussian motion, while for restricted anomalous diffusion, a more general power law applies.[47,48]

The $^1$H DOSY map of NG-based bijel, as shown in Figure 5b, clearly indicates the presence of two distinct diffusing species ascribed to the organic phase/water solution. The diffusion coefficient of water in bijels was $D_w = 2.7 \times 10^{-9}$ m$^2$/s, consistent with literature data for free water solutions at 305 K.[49] The organic phase (PCL) exhibits a slower motion with a $D_{PCL}$ value of $8.9 \times 10^{-11}$ m$^2$/s. Moreover, DOSY experiments carried out at variable observation time $\Delta$ in the range of 10−60 ms show a linear regression of the MSD versus $\Delta$ for the


https://doi.org/10.1021/acsomega.2c04834
ACS Omega 2022, 7, 42845−42853

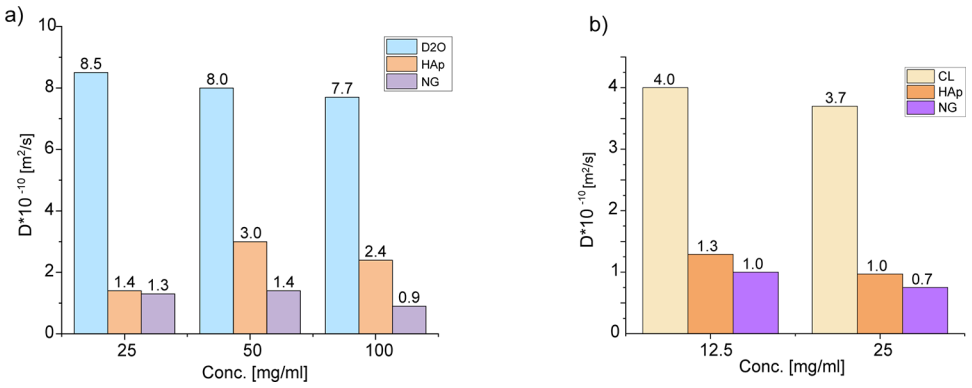


**Figure 6.** Diffusion coefficients measured via $^1$H DOSY NMR at 305 K of (a) ethosuximide dissolved in $D_2O$ and loaded in HAp- and NG-based bijels; (b) dimethyl fumarate dissolved in caprolactone (CL) and loaded in HAp- and NG-based bijels. The experimental data are estimated to be accurate about ±2 to 10%.

diffusing water molecules (see Figure S6, Supporting Information). This is consistent with the diffusion process being Gaussian and unrestricted over the length scale $l_D$ accessible by DOSY NMR experiments. The observed diffusion length scale, within which $l_D = (2D\Delta)^{1/2}$ covers the range of 7−18 $\mu$m, ensures the bicontinuous structure of the gels. Similar results were obtained for NG- and HAp-based bijels when loaded with the two drugs, ethosuximide and dimethyl fumarate in the water/organic phase, thus ensuring that the bicontinuous structure consisting of two immiscible domains is maintained even after drug loading.

Furthermore, the diffusion coefficient of ethosuximide and dimethyl fumarate loaded in both bijel/HAp and bijel/NG at different drug concentrations has been measured and the data are reported in Figure 6 together with the drug diffusion in pure water/organic solution for comparison. The results indicate that the diffusivity of the drugs in both bijel formulations is always slower than in free aqueous/organic solutions for all the concentrations, thus indicating the presence of confined diffusion within the bijel interconnected domains. Specifically, the decrease in diffusivity seems to become more distinct for the bijels stabilized with nanogel nanoparticles.

The diffusion motion through bicontinuous structures and porous materials is known to depend on the microstructural topology[50,51] usually described by the porosity, $\phi$, and tortuosity, $\tau$. Tortuosity is related to the distribution and interconnectivity of the pores or domains that may prolong the diffusional pathways and therefore limit the molecular motion over length scales even larger than the pore/domain sizes. Moreover, additional interactions of the drug molecules with the nanoparticle surface can modify their transport properties properly described by an effective diffusion coefficient, $D_{eff}$, lower than the diffusion in the bulk solvent, $D_0$. The parameter $\tau_{eff}$ defined as the ratio of $D_{eff}$ over $D_0$ reflects both the geometric tortuosity of the bijel structure and the nanoparticle surface-drug interactions.[52] Table 1 collects the values of $\tau_{eff}$, obtained from the diffusion data of Figure 6, for all our systems.

Clearly, a reduction of the diffusion coefficient relative to its value $D_0$, due to geometric tortuosity and physico-chemical interactions, is specific for each drug type/concentration and nanoparticle used in the bijel formulation. At the lower ethosuximide concentration, $\tau_{eff}$ is similar in both bijel formulations, while as the drug concentration increases, $\tau_{eff}$ is lower for bijel/NG than that for bijel/HAp, indicating both the presence of more convoluted domains and/or stronger drug−nanoparticle interactions in the 3D bijel/NG network. Similarly, dimethyl fumarate in bijel/NG formulation also shows lower $\tau_{eff}$ values regardless of drug concentration. These results suggest that the tortuosity and interactions induced by the two bijel formulations are different and affect the drug motion in the millisecond time scale.

**Table 1. Values of $\tau_{eff}$ for Ethosuximide and Dimethyl Fumarate in the Two Bijel Formulations**

| C[mg/mL] | $\tau_{eff}$ (bijel/HAp) | $\tau_{eff}$ (bijel/NG) |
|---|---|---|
| | Ethosuximide | |
| C1 (25) | 0.16 | 0.15 |
| C2 (50) | 0.37 | 0.17 |
| C3 (100) | 0.31 | 0.11 |
| | Dimethyl fumarate | |
| C4 (12.5) | 0.32 | 0.25 |
| C5 (25) | 0.27 | 0.19 |

**3.2. Release Kinetics.** Two aqueous hydrophilic drug mimetics, namely, rhodamine B (RhB) and sodium fluorescein (SF), have been selected due to their similarity to many analgesic and anti-inflammatory drugs.[32] The release profiles of these model compounds can be observed in Figure 7. As far as RhB is concerned, no substantial differences in the cumulative release can be noticed, while for SF, some discrepancies are present when shifting from the HAp to the NG bijel formulations. However, these differences will not be discussed in detail since these results are only reported as reference. It is worth mentioning that rhodamine B is a cationic species, while the fluorescein molecule has negative charges, so we can evaluate the effect of the molecular charges on the release kinetics. A sustained release was observed for both compounds. The different rates and extents of SF release can be due to the presence of SF-NG nanoparticle non-covalent interactions.

Once the procedure has been optimized on SF and RhB, the release kinetics of ethosuximide and dimethyl fumarate has been performed. Figure 8 shows their cumulative release as a function of time.

Initial burst releases of 25 and 17% were observed after 30 min for ethosuximide released from bijel/HAp and bijel/NP, respectively; after that, a sustained drug release was observed. The initial burst release is due to the drug molecules located on the particle surface or to a possible aggregation, while the drug included in the bijel mesoscopic domains was released in


https://doi.org/10.1021/acsomega.2c04834
ACS Omega 2022, 7, 42845−42853

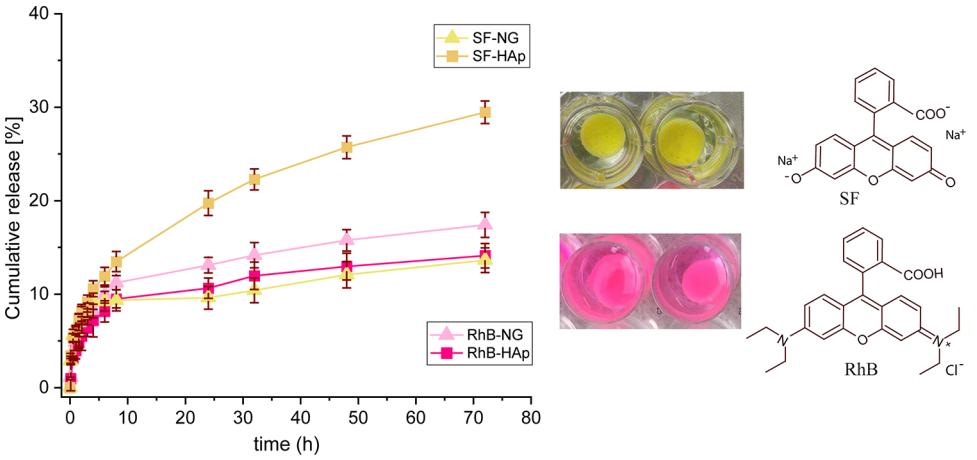


**Figure 7.** *In vitro* release profiles of SF and RhB from bijel/HAp and bijel/NG in the time range of 0−72 h. The chemical structure of SF and RhB molecules is also shown. Data SF-HAp are taken from ref 32.

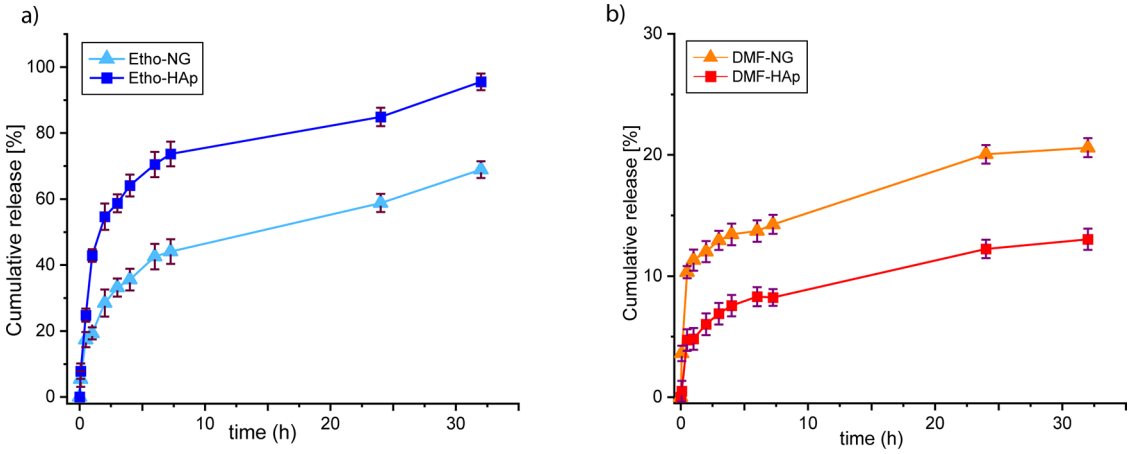


**Figure 8.** *In vitro* release profiles of (a) ethosuximide and (b) dimethyl fumarate from bijel/HAp and bijel/NG in the time range of 0−32 h.

a prolonged manner. Similarly to what was observed for fluorescein, the presence of NG nanoparticles significantly decreases the percentage of the drug released, and after 32 h, the cumulative amount of ethosuximide released by bijel/NG is 69% compared to 95% by bijel/HAp. The slow release kinetics can be attributed to drug-NG nanoparticle interactions that prevent the drug from moving away from the bijel matrix. These results are consistent with a slower drug diffusion in the bijel/NG measured in the NMR time scale. Conversely, the release profile of dimethyl fumarate (Figure 8b) is very slow over time and only 13% (bijel/HAp) and 20% (bijel/NG) of the drug were released within 32 h due to the lower affinity of DMF for the aqueous solution. In this case, the presence of the nanogel nanoparticles in the porous structure induces a slightly faster release kinetics of DMF. Overall, these results highlight that the bijel structure/nanoparticles have an impact on the macroscopic release and could be used to prolong the effect of the medicine.

To further investigate the drug release mechanism from bijels, the experimental release profile $f_t$ (up to 60% cumulative release) for both drugs and bijel formulations was analyzed using the Korsmeyer−Peppas model:[53−55]

$$f_t = \frac{M_t}{M_\infty} = kt^n \quad (3)$$

where $k$ is a constant, $M_t$ and $M_\infty$ are the fractions of the drug released at time $t$ and at infinite time, respectively, and $n$ is the diffusion exponent indicative of the drug transport mechanism. The fitting results are summarized in Table 2; all values of $n$ are lower than 0.45, thus suggesting that Fickian diffusion drives the drugs released from both bijel formulations. For all data sets, the correlation coefficient ($R^2$) was rather high (min. 0.96 up to 0.98; data are shown in the Supporting Information, Figures S7 and S8). A similar release profile from bijels has also been reported for drug-like molecules[31] and by Singh and Kumar[56] for moxifloxacin, in which the mechanism of drug release also followed the Fickian diffusion.

**Table 2. Parameters ($k$ and $n$) Obtained by Fitting the Drug Release Data**

| sample | $k$ | $n$ |
|---|---|---|
| etho-bijel/NG | 38.49 | 0.439 |
| etho-bijel/HAp | 22.17 | 0.323 |
| DMF-bijel/NG | 10.05 | 0.209 |
| DMF-bijel/HAp | 4.78 | 0.295 |

## 4. CONCLUSIONS

Biphasic water/oil porous structures have been successfully prepared and characterized. In these systems, fluid−fluid



https://doi.org/10.1021/acsomega.2c04834
ACS Omega 2022, 7, 42845−42853

interfaces were stabilized by either hydroxyapatite (inorganic) or nanogel (organic) nanoparticles. The microstructures of such materials and nanoparticle surface interactions play a key role in the mass transport of small molecules such as active ingredients through the tortuous biphasic domains. The diffusion coefficients of the drugs in the bijel network, measured with HR-MAS NMR techniques, are reduced compared to diffusion in bulk solution, and this reduction depends on both the type of nanoparticles and drug concentration.

Furthermore, the *in vitro* release study showed sustained release of both ethosuximide and dimethyl fumarate from bijel structures, which followed the Fickian mechanism of diffusion despite the effect of the drug−nanoparticle non-covalent interactions that modify the amount of drug released over time. The microstructure/nanoparticle type allows us to design the desired properties of these materials as multi-drug delivery systems.

## ■ ASSOCIATED CONTENT

### Supporting Information

The Supporting Information is available free of charge at https://pubs.acs.org/doi/10.1021/acsomega.2c04834.

DSC plot, DLS analysis, NMR spectra of DMF, dynamics of $H_2O$ in bijels, and release data analysis (PDF)

## ■ AUTHOR INFORMATION


### Corresponding Authors

**Filippo Rossi** − *Department of Chemistry, Materials and Chemical Engineering "G. Natta", Politecnico di Milano, 20133 Milano, Italy*; orcid.org/0000-0003-2665-120X; Phone: +390223993145; Email: filippo.rossi@polimi.it

**Franca Castiglione** − *Department of Chemistry, Materials and Chemical Engineering "G. Natta", Politecnico di Milano, 20133 Milano, Italy*; orcid.org/0000-0003-2413-8808; Phone: +390223993193; Email: franca.castiglione@polimi.it

### Authors

**Valeria Vanoli** − *Department of Chemistry, Materials and Chemical Engineering "G. Natta", Politecnico di Milano, 20133 Milano, Italy*

**Giovanna Massobrio** − *Department of Chemistry, Materials and Chemical Engineering "G. Natta", Politecnico di Milano, 20133 Milano, Italy*

**Fabio Pizzetti** − *Department of Chemistry, Materials and Chemical Engineering "G. Natta", Politecnico di Milano, 20133 Milano, Italy*

**Andrea Mele** − *Department of Chemistry, Materials and Chemical Engineering "G. Natta", Politecnico di Milano, 20133 Milano, Italy; CNR Istituto di Chimica del Riconoscimento Molecolare, 20131 Milan, Italy*; orcid.org/0000-0002-0351-0538

Complete contact information is available at: https://pubs.acs.org/10.1021/acsomega.2c04834


### Notes

The authors declare no competing financial interest.

## ■ ACKNOWLEDGMENTS

Authors would like to thank Prof. Maurizio Masi for fruitful discussion.

## ■ REFERENCES


(1) Stratford, K.; Adhikari, R.; Pagonabarraga, I.; Desplat, J.-C.; Cates, M. E. Colloidal jamming at interfaces: A route to fluid-bicontinuous gels. *Science* **2005**, *309*, 2198−2201.

(2) Cates, M. E.; Clegg, P. S. Bijels: a new class of soft materials. *Soft Matter* **2008**, *4*, 2132−2138.

(3) Herzig, E. M.; White, K. A.; Schofield, A. B.; Poon, W. C. K.; Clegg, P. S. Bicontinuous emulsions stabilized solely by colloidal particles. *Nat. Mater.* **2007**, *6*, 966−971.

(4) Tavacoli, J. W.; Thijssen, J. H. J.; Schofield, A. B.; Clegg, P. S. Novel, robust, and versatile bijels of nitromethane, ethanediol, and colloidal silica: capsules, subten-micrometer domains, and mechanical properties. *Adv. Funct. Mater.* **2011**, *21*, 2020−2027.

(5) Lee, M. N.; Mohraz, A. Bicontinuous macroporous materials from bijel templates. *Adv. Mater.* **2010**, *22*, 4836−4841.

(6) Levesque, S. G.; Lim, R. M.; Shoichet, M. S. Macroporous interconnected dextran scaffolds of controlled porosity for tissue-engineering applications. *Biomaterials* **2005**, *26*, 7436−7446.

(7) Martina, M.; Subramanyam, G.; Weaver, J. C.; Hutmacher, D. W.; Morse, D. E.; Valiyaveettil, S. Developing macroporous bicontinuous materials as scaffolds for tissue engineering. *Biomaterials* **2005**, *26*, 5609−5616.

(8) Cai, D.; Clegg, P. S.; Li, T.; Rumble, K. A.; Tavacoli, J. W. Bijels formed by direct mixing. *Soft Matter* **2017**, *13*, 4824−4829.

(9) Witt, J. A.; Mumm, D. R.; Mohraz, A. Microstructural tunability of cocontinuous bijel-derived electrodes to provide high energy and power densities. *J. Mater. Chem. A* **2016**, *4*, 1000−1007.

(10) Lupi, F. R.; Shakeel, A.; Greco, V.; Rossi, C. O.; Baldino, N.; Gabriele, D. A rheological and microstructural characterisation of bigels for cosmetic and pharmaceutical uses. *Mater. Sci. Eng. C.* **2016**, *69*, 358−365.

(11) Lupi, F. R.; Gentile, L.; Gabriele, D.; Mazzulla, S.; Baldino, N.; de Cindio, B. Olive oil and hyperthermal water bigels for cosmetic uses. *J. Colloid Interface Sci.* **2015**, *459*, 70−78.

(12) Andonova, V.; Peneva, P.; Georgiev, G. S.; Toncheva, V. T.; Apostolova, E.; Peychev, Z.; Dimitrova, S.; Katsarova, M.; Petrova, N.; Kassarova, M. Ketoprofen-loaded polymer carriers in bigel formulation: An approach to enhancing drug photostability in topical application forms. *Int. J. Nanomed.* **2017**, *12*, 6221−6238.

(13) Ivaskiene, M.; Mazurkeviciute, A.; Ramanauskiene, K.; Ivaskiene, M.; Grigonis, A.; Briedis, V. Topical antifungal bigels: Formulation, characterization and evaluation. *Acta Pharm.* **2018**, *68*, 223−233.

(14) Hamed, R.; Mahmoud, N. N.; Alnadi, S. H.; Alkilani, A. Z.; Hussein, G. Diclofenac diethylamine nanosystems-loaded bigels for topical delivery: development, rheological characterization, and release studies. *Drug Dev. Ind. Pharm.* **2020**, *46*, 1705−1715.

(15) Martín-Illana, A.; Notario-Pérez, F.; Cazorla-Luna, R.; Ruiz-Caro, R.; Bonferoni, M. C.; Tamayo, A.; Veiga, M. D. Bigels as drug delivery systems: From their components to their applications. *Drug Discovery Today* **2022**, *27*, 1008−1026.

(16) Murdan, S. Organogels in drug delivery. *Expert Opin. Drug Delivery* **2005**, *2*, 489−505.

(17) Esposito, C. L.; Kirilov, P.; Roullin, V. G. Organogels, promising drug delivery systems: an update of state-of-the-art and recent applications. *J. Controlled Release* **2018**, *271*, 1−20.

(18) Zhang, Y.; Khademhosseini, A. Advances in engineering hydrogels. *Science* **2017**, *356*, eaaf3627.

(19) Peppas, N. A.; Bures, P.; Leobandung, W.; Ichikawa, H. Hydrogels in pharmaceutical formulations. *Eur. J. Pharm. Biopharm.* **2000**, *50*, 27−46.

(20) Dreiss, C. A. Hydrogel design strategies for drug delivery. *Curr. Opin. Colloid Interface Sci.* **2020**, *48*, 1−17.

(21) Welch, P. M.; Lee, M. N.; Parra-Vasquez, A. N. G.; Welch, C. F. Jammed limit of bijel structure formation. *Langmuir* **2017**, *33*, 13133−13138.
(22) Cui, M.; Miesch, C.; Kosif, I.; Nie, H.; Kim, P. Y.; Kim, H.; Emrick, T.; Russel, T. P. Transition in dynamics as nanoparticles jam at the liquid/liquid interface. *Nano Lett.* **2017**, *17*, 6855−6862.
(23) Boeker, A.; He, J.; Emrick, T.; Russell, T. P. Self-assembly of nanoparticles at interfaces. *Soft Matter* **2007**, *3*, 1231−1248.
(24) Haase, M. F.; Stebe, K. J.; Lee, D. Continuous fabrication of hierarchical and asymmetric bijel microparticles, fibers, and membranes by Solvent Transfer-Induced Phase Separation (STRIPS). *Adv. Mater.* **2015**, *27*, 7065−7071.
(25) Russell, J. T.; Lin, Y.; Boeker, A.; Su, L.; Carl, P.; Zett, H.; He, J.; Sill, K.; Tangirala, R.; Emrick, T.; Littrell, K.; Thiyagarajan, P.; Cookson, D.; Fery, A.; Wang, Q.; Russell, T. P. Self-assembly and cross-linking of bionanoparticles at liquid−liquid interfaces. *Angew. Chem., Int. Ed.* **2005**, *44*, 2420−2426.
(26) Jansen, F.; Harting, J. From bijels to Pickering emulsions: A lattice Boltzmann study. *Phys. Rev. E* **2011**, *83*, 046707.
(27) Arabjamaloei, R.; Shah, R. S.; Bryant, S.; Trifkovic, M. Controlling structure of materials derived from spinodally decomposing liquids. *Phys. Fluids* **2021**, *33*, 032020.
(28) Carmack, J.; Millet, P. C. Numerical simulations of bijel morphology in thin films with complete surface wetting. *J. Chem. Phys.* **2015**, *143*, 154701.
(29) Cai, D.; Clegg, P. S. Stabilizing bijels using a mixture of fumed silica nanoparticles. *Chem. Commun.* **2015**, *51*, 16984−16987.
(30) Bai, L.; Fruehwirth, J. W.; Cheng, X.; Macosko, C. W. Dynamics and rheology of nonpolar bijels. *Soft Matter* **2015**, *11*, 5282−5293.
(31) Hijnen, N.; Cai, D.; Clegg, P. S. Bijels stabilized using rod-like particles. *Soft Matter* **2015**, *11*, 4351−4355.
(32) Pizzetti, F.; Rossetti, A.; Marchetti, A.; Castiglione, F.; Vanoli, V.; Coste, E.; Veneruso, V.; Veglianese, P.; Sacchetti, A.; Cingolani, A.; Rossi, F. Bicontinuous structures formed by monomer/water interface stabilization with colloidal nanoparticles. *Adv. Mater. Interfaces* **2021**, *8*, 210091.
(33) Gören, M. Z.; Onat, F. Ethosuximide: from bench to bedside. *CNS Drug Rev.* **2007**, *13*, 224−239.
(34) Blair, H. A. Dimethyl fumarate: a review in moderate to severe plaque psoriasis. *Drugs* **2018**, *78*, 123−130.
(35) Burness, C. B.; Deeks, E. D. Dimethyl fumarate: a review of its use in patients with relapsing-remitting multiple sclerosis. *CNS Drugs* **2014**, *28*, 373−387.
(36) Santoro, M.; Marchetti, P.; Rossi, F.; Perale, G.; Castiglione, F.; Mle, A.; Masi, M. Smart approach to evaluate drug diffusivity in injectable agar-carbomer hydrogels for drug delivery. *J. Phys. Chem. B* **2011**, *115*, 2503−2510.
(37) Kimmich, R.*Principles of Soft-Matter Dynamics*. Springer, London, 2012.
(38) Jenkins, J. E.; Hibbs, M. R.; Alam, T. M. Identification of multiple diffusion rates in mixed solvent anion exchange membranes using high resolution MAS NMR. *ACS Macro Lett.* **2012**, *1*, 910−914.
(39) Perale, G.; Rossi, F.; Santoro, M.; Marchetti, P.; Mele, A.; Castiglione, F.; Raffa, E.; Masi, M. Drug release from hydrogel: a new understanding of transport phenomena. *J. Biomed. Nanotechnol.* **2011**, *7*, 476−481.
(40) Ferro, M.; Castiglione, F.; Punta, C.; Melone, L.; Panzeri, W.; Rossi, B.; Trotta, F.; Mele, A. Anomalous diffusion of Ibuprofen in cyclodextrin nanosponges hydrogels: an HRMAS NMR study. *Beilstein J. Org. Chem.* **2014**, *10*, 2580−2593.
(41) Kumar, R.; Prakash, K. H.; Cheang, P.; Khor, K. A. Temperature driven morphological changes of chemically precipitated hydroxyapatite nanoparticles. *Langmuir* **2004**, *20*, 5196−5200.
(42) Marino, A.; Arai, S.; Hou, Y.; Pellegrino, M.; Mazzolai, B.; Mattoli, V.; Suzuki, M.; Ciofani, G.Assessment of the effects of a wireless neural stimulation mediated by piezoelectric nanoparticles. In: Santamaria, F., Peralta, X. (eds) *Use of Nanoparticles in Neuroscience. Neuromethods*2018, *135*Humana Press, New York, NY.
(43) Pelta, M. D.; Barjat, H.; Morris, G. A.; Davis, A. L.; Hammond, S. J. Pulse sequences for high-resolution diffusion-ordered spectroscopy (HR-DOSY). *Magn. Reson. Chem.* **1998**, *36*, 706−714.
(44) Zubkov, M.; Dennis, G. R.; Stait-Gardner, T.; Torres, A. M.; Willis, S. A.; Zheng, G.; Price, W. S. Physical characterization using diffusion NMR spectroscopy. *Magn. Reson. Chem.* **2017**, *55*, 414−424.
(45) Groves, P. Diffusion ordered spectroscopy (DOSY) as applied to polymers. *Polym. Chem.* **2017**, *8*, 6700−6708.
(46) Fiorati, A.; Negrini, N. C.; Baschenis, E.; Altomare, L.; Faré, S.; Schieroni, A. G.; Piovani, D.; Mendichi, R.; Ferro, M.; Castiglione, F.; Mele, A.; Punta, C.; Melone, L. TEMPO-nanocellulose/$Ca^{2+}$ hydrogels: Ibuprofen drug diffusion and in vitro cytocompatibility. *Materials* **2020**, *13*, 183−199.
(47) Phillies, G. Diffusion on a molecular scale as observed using PGSE NMR. *Concepts Magn. Reson., Part A* **2015**, *44*, 1−15.
(48) Castiglione, F.; Casalegno, M.; Ferro, M.; Rossi, F.; Raos, G.; Mele, A. Evidence of superdiffusive nanoscale motion in anionic polymeric hydrogels: Analysis of PGSE- NMR data and comparison with drug release properties. *J. Controlled Release* **2019**, *305*, 110−119.
(49) Holz, M.; Heil, S. R.; Sacco, A. Temperature-dependent self-di†usion coefficients of water and six selected molecular liquids for calibration in accurate $^1$H NMR PFG measurements. *Phys. Chem. Chem. Phys.* **2000**, *2*, 4740−4742.
(50) McDevitt, K. M.; Thorson, T. J.; Botvinick, E. L.; Mumm, D. R.; Mohraz, A. Microstructural characteristics of bijel-templated porous materials. *Materialia* **2019**, *7*, 100393.
(51) Shen, L.; Chen, Z. Critical review of the impact of tortuosity on diffusion. *Chem. Eng. Sci.* **2007**, *62*, 3748−3755.
(52) Rottreau, T. J.; Parlett, C. M. A.; Lee, A. F.; Evans, R. Diffusion NMR characterization of catalytic silica supports: a tortuous path. *J. Phys. Chem. C* **2017**, *121*, 16250−16256.
(53) Ritger, P. L.; Peppas, N. A. A simple equation for description of solute release II Fickian and anomalous release from swellable devices. *J. Controlled Release* **1987**, *5*, 37−42.
(54) Korsmeyer, R. W.; Gurny, R.; Doelker, E.; Buri, P.; Peppas, N. A. Mechanisms of solute release from porous hydrophilic polymers. *Int. J. Pharm.* **1983**, *15*, 25−35.
(55) Peppas, N. A.; Narasimhan, B. Mathematical models in drug delivery: How modeling has shaped the way we design new drug delivery systems. *J. Controlled Release* **2014**, *190*, 75−81.
(56) Singh, B.; Kumar, R. Designing biocompatible sterile organogel−bigel formulations for drug delivery applications using green protocol. *New J. Chem.* **2019**, *43*, 3059−3070.


https://doi.org/10.1021/acsomega.2c04834
*ACS Omega* 2022, 7, 42845−42853